ACS APPLIED POLYMER MATERIALS

pubs.acs.org/acsapm
Article

Multiresponsive Glutathione-Functionalized Waterborne Polyurethane/PEDOT System for Electrically and Redox-Controlled Delivery of an Anticancer Peptide

Francesco Cancilla, Fabio Salvatore Palumbo, Calogero Fiorica, Giovanna Pitarresi, Maria M. Pérez-Madrigal, Carlos Alemán, and Leonor Resina*

Cite This: *ACS Appl. Polym. Mater.* 2026, 8, 8479–8494

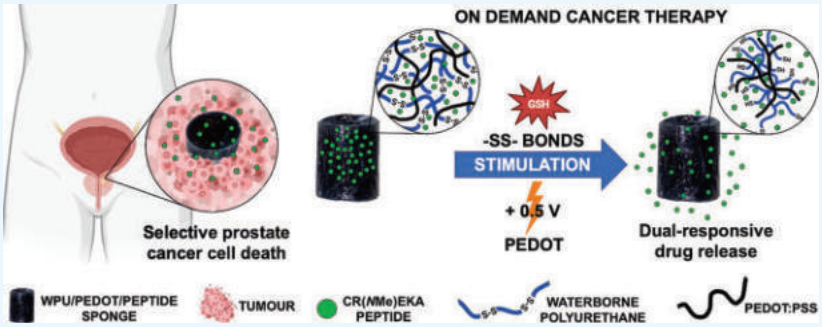

ABSTRACT: Prostate cancer remains one of the leading causes of cancer-related mortality. Although there were advances in cancer therapy, there is a need for advanced drug delivery strategies to improve the spatiotemporal control of therapeutic action. Here, we developed conductive, redox-responsive hybrid sponges based on glutathione-extended waterborne polyurethane (WPU-GSSG) and the electroactive polymer poly(3,4-ethylenedioxythiophene) (PEDOT) for dual-stimuli-triggered release of anticancer peptide in locoregional tumor therapy. WPU/PEDOT porous scaffolds presented lightweight and mechanically resilient structures with homogeneous loading of the pentapeptide Cys-Arg-*N*-methyl-Glu-Lys-Ala (CR(*N*Me)EKA). PEDOT incorporation significantly enhanced the electrochemical properties of the sponges, providing reversible redox activity, reduced impedance, and near-ideal capacitive behavior. The sponges supported cell adhesion and high cell viability within the three-dimensional architecture. In vitro release studies demonstrated that peptide delivery is regulated by a synergistic combination of redox and electrical stimuli. A mimetic tumor microenvironment accelerated peptide release relative to physiological conditions. Electrostimulation (+0.5 V chronoamperometry) further enhanced release kinetics, and the combined application of redox and electrical triggers enabled peptide release of up to ∼94%, demonstrating tunable stimulus-responsive delivery. Functional assays on cancer cells supported the therapeutic potential of this platform. While WPU alone was fully cytocompatible and PEDOT-containing sponges exhibited moderate electrostimulation-dependent effects, CR(*N*Me)EKA-loaded conductive sponges induced a pronounced reduction in cancer cell viability under electrostimulation, decreasing survival to ∼20%. Although further in vivo validation is required, these findings highlight the potential of multifunctional WPU/PEDOT sponges for localized, stimuli-responsive peptide delivery.

KEYWORDS: *prostate cancer, polyurethane, PEDOT, redox, electrostimulation, locoregional drug delivery*

1. INTRODUCTION

Prostate cancer remains one of the most prevalent malignancies among men worldwide and is a leading cause of cancer-related morbidity and mortality.[1,2] Although advances in surgery, radiotherapy, hormonal therapy, and chemotherapy have improved patient outcomes, therapeutic efficacy is frequently limited by insufficient tumor selectivity, systemic toxicity, and the development of drug resistance.[2] Many anticancer agents require high systemic doses to achieve effective intratumoral concentrations, resulting in dose-limiting side effects and a reduced quality of life.[1,3,4] These limitations have driven a growing interest in advanced drug delivery strategies capable of improving the spatial and temporal control of therapeutic action.[5,6]

Stimuli-responsive biomaterials have emerged as a powerful approach to address these challenges by exploiting the

Received: March 6, 2026
Revised: May 15, 2026
Accepted: May 18, 2026
Published: May 21, 2026

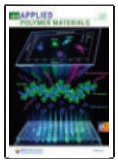

https://doi.org/10.1021/acsapm.6c00875
ACS Appl. Polym. Mater. 2026, 8, 8479–8494

distinctive biochemical and physicochemical features of the tumor microenvironment (TME).[7−9] The hallmarks of solid tumors include extracellular acidity, elevated glutathione (GSH) levels, oxidative stress, hypoxia, and aberrant vasculature, all of which can be leveraged to trigger selective drug release.[10−13] Among endogenous stimuli, redox responsiveness is particularly attractive since GSH levels are markedly elevated in cancer, both within tumor cells and in the surrounding TME, compared to healthy tissues. This redox imbalance provides a robust trigger for the activation of delivery systems incorporating reducible or GSH-sensitive moieties, enabling enhanced selectivity and reduced off-target effects.[14−17]

In parallel, externally applied stimuli can offer additional and complementary levels of control. Electrical stimulation is particularly appealing due to its reversibility, precise temporal control, and compatibility with implantable or wearable devices.[12,18] Conductive polymers, such as poly(3,4-ethylenedioxythiophene)/poly(styrenesulfonate) (PEDOT/PSS), undergo reversible redox transitions under mild electrical potentials, leading to changes in polymer conformation, charge density, and polymer−cargo interactions.[19] These properties have been successfully exploited to achieve on-demand, electrically triggered release of drugs and biomolecules.[20−23] Importantly, electrical stimulation can be applied locally and repeatedly using low voltages, making it well-suited for biomedical interfaces.[24,25]

The integration of endogenous and exogenous responsiveness within a single material platform represents a promising strategy for enhancing therapeutic precision. Multiresponsive systems can autonomously respond to tumor-specific biochemical cues while remaining amenable to external modulation, allowing programmable dosing and timing.[12,18] Previous studies on electro responsive and dual-stimulus systems have demonstrated that combining multiple triggers can overcome the limitations of single-responsive carriers and improve release kinetics and therapeutic efficacy.[20−23]

Peptide-based therapeutics are particularly attractive for cancer treatment due to their high specificity and potent activity. However, their clinical translation is often hindered by rapid proteolytic degradation, limited stability, and poor retention within tumor tissues, necessitating advanced delivery strategies. For instance, the tumor-homing pentapeptide CREKA, and its *N*-methylated analog CR(*N*Me)EKA, demonstrate pronounced antitumor activity in prostate cancer models but face intrinsic limitations due to their small size and hydrophilicity, requiring a robust delivery system for protection and controlled release.[23,26]

While multiresponsive systems offer superior control, their development for delicate peptide therapeutics, particularly those requiring protection from degradation and precise, on-demand release in complex biological environments, presents a formidable challenge. Specifically, there is a critical need for integrated platforms that can simultaneously protect potent anticancer peptides like CR(*N*Me)EKA, provide tumor-specific release via endogenous cues, and allow for external, programmable modulation to optimize therapeutic outcomes.

To address this critical need for an integrated platform, we have developed a novel multiresponsive system utilizing elastomeric waterborne polyurethane (WPU) with intrinsic glutathione-responsiveness and externally addressable electroconductivity via PEDOT/PSS, as a versatile and biocompatible framework.[27] WPUs are particularly well-suited for small, hydrophilic peptides like CR(*N*Me)EKA, offering a protective matrix and enabling controlled release. Their segmented architecture allows fine control over properties, while their aqueous synthesis preserves peptide integrity. We further engineered these WPUs by incorporating glutathione-derived chain extenders to introduce intrinsic responsiveness to reductive environments, enabling selective activation within GSH-rich intracellular compartments.[27−29] Simultaneously, embedding conductive PEDOT/PSS into the WPU matrix confers electro responsiveness, allowing externally triggered modulation of release.

Building on these unmet needs, this study aims to develop and characterize a novel multiresponsive delivery platform based on a glutathione-functionalized WPU integrated with PEDOT/PSS for the controlled delivery of the anticancer peptide CR(*N*Me)EKA. By combining endogenous redox sensitivity with externally applied electrical stimulation, this system enables the programmable and on-demand modulation of peptide release while maintaining stability under physiological conditions. This work focuses on the synthesis, physicochemical and electrochemical characterization of the WPU/PEDOT/PSS matrix, as well as its peptide-loading capacity and release profiles under reductive and electrically stimulated conditions, with the goal of establishing a soft, electrically addressable, and redox-responsive polymer interface for advanced cancer therapies.

2. MATERIALS AND METHODS

2.1. Materials

Poly(ethylene glycol) (PEG Mw 1000), ε-caprolactone (ε-CL), L-glutathione oxidized (GSSG), toluene, diethyl ether, isopropanol, CaH_2, stannous octoate, sodium chloride (NaCl) and triethyl-amine (TEA) were acquired from Sigma-Aldrich srl (Italy). Methyl-ethyl ketone (MEK), 2,2-bis(hydroxymethyl)propionic acid (DMPA), isophorone diisocyanate (IPDI) and acetic acid were acquired from Fisher Scientific Italia. Dulbecco's phosphate buffered saline (DPBS), PEDOT/PSS dispersion Clevios PH 1000 (PEDOT/PSS ratio of 1:2.5, solids content 1.0−1.3%), and DL-dithiothreitol (DTT) were acquired from Sigma-Aldrich (Germany), and the CR(*N*Me)EKA peptide was acquired from Biomatik (Canada). Materials for biological experiments were acquired from Thermo Fisher Scientific (USA).

2.2. Synthesis of Glutathione-Extended Waterborne Polyurethane (WPU-GSSG)

Glutathione-extended waterborne polyurethane (WPU-GSSG) was synthesized following a previously reported procedure.[27] Briefly, PCL-PEG-PCL (2225 mg) and 2,2-bis(hydroxymethyl)propionic acid (DMPA, 110.5 mg) were melted at 70 °C under stirring (180 rpm) with an overhead paddle stirrer. Isophorone diisocyanate (0.475 mL) was then added dropwise, and the reaction was allowed to proceed for 3 h under an argon atmosphere, using stannous octoate as the catalyst. Subsequently, methyl ethyl ketone (MEK, 2.5 mL) was introduced to reduce the viscosity, and the carboxylic acid groups were neutralized with triethylamine (TEA). An aqueous solution of GSSG (606 mg in 17.5 mL of distilled water) was then added, and the mixture was emulsified under vigorous stirring at room temperature for 20 h. After removal of MEK by rotary evaporation, the resulting WPU-GSSG derivative was purified by exhaustive dialysis (2 days against ultrapure water containing NaCl, followed by 4 days against ultrapure water). Finally, the aqueous WPU dispersion was freeze-dried.

2.3. Fabrication of WPU/PEDOT Sponge

900 mg of WPU-GSSG were dispersed in PEDOT/PSS Clevios PH 1000 at a concentration of 10% w/v by autoclaving. Subsequently, the dispersion was poured into cylindrical molds (9 mm in diameter), frozen at −80 °C and lyophilized to obtain the final sponge. Blank

https://doi.org/10.1021/acsapm.6c00875
ACS Appl. Polym. Mater. 2026, 8, 8479−8494

sponges were fabricated following the same procedure, dispersing 900 mg of WPU-GSSG in distilled water (10% w/v) instead of PEDOT/PSS.

2.4. Swelling and Degradation Studies

Sponges (mean weight of 30 mg, 9 mm in diameter, 4 mm in height) after lyophilization were weighed (W_0) and incubated at 37 °C in 1 mL of DPBS at pH 7.4, without and with the addition of DTT 10 mM. The swelling behavior of the sponges was monitored for up to 60 days; at each time point, samples were weighed after gently removing excess water with soft filter paper (W_S). The swelling ratio (Q_{SW}) was calculated using the following equation

$$Q_{SW} = \frac{W_S}{W_0}$$

where W_0 is the dry weight of samples and W_S is the weight of samples after swelling. The analyses were carried out in triplicate (n = 3) after 5, 30 min, 1, 2, 6 h, 1, 2, 3, 7, 15, 30, and 60 days.

The hydrolysis study was investigated for up to 120 days. The analyses were carried out in triplicate (n = 3) at 1, 2, 3, 7, 15, 30, 60, 90, and 120 days and the medium was replaced weekly. At each time point, samples were washed in distilled water, lyophilized and weighed.

Hydrolytic degradation was expressed as residual weight percentage ($W_{R\%}$), calculated as the ratio between the weight of the sample at time t_n (W_n) and the weight of the sample at time t_0 (W_0)

$$W_{R\%} = (W_n / W_0) \times 100$$

2.5. Microstructural Characterization

Porosity and internal architecture of the sponges were determined by microcomputed tomography (micro-CT) analysis using a Skyscan 1272 Bruker equipment (Kontich, Belgium). Reconstruction of the 360 cross-section images representing the middle of the samples was conducted using the NRecon 1.7.0.4 software (Bruker micro-CT, Kontich, Belgium), and 3D visualizations were achieved using DataViewer and CTVox (Bruker micro-CT, Belgium). Porosity and pore diameter were assessed using the CTAnalyser 1.16.9.0 software (Bruker micro-CT, Kontich, Belgium), which determines porosity within the selected 3D volume of interest. Morphometric parameters, including structure thickness (St.Th) and structure separation (St.Sp, used as a measure of pore size), were calculated using 3D model-independent methods. Furthermore, the volumetric pore size distribution was extracted to evaluate the structural heterogeneity and the presence of anisotropic features. Measurements were performed at a source voltage of 50 kV, a source current of 200 μA, 3 μm pixel size and 180° rotation.

2.6. Mechanical Characterization

Compression tests on sponges were carried out on dried and swollen samples. Swollen samples were equilibrated in DPBS at 37 °C for 24 h before testing. Cylindrical sponge specimens (9 mm in diameter, 12 mm in height) were carefully placed between the compression platens, ensuring parallel alignment and uniform surface contact. A preload force of 0.05 N was applied, and uniaxial compression was conducted at a crosshead speed of 10 mm/min. Cyclic compression tests were performed on swollen sponge samples to evaluate their mechanical resilience. Samples were subjected to repeated static compression−relaxation cycles (5 cycles) under different strain levels (20%, 40%, and 60%). All compression measurements were performed in sextuplicate (n = 6) at room temperature. Compression tests were conducted using the Shimadzu EZ-LX universal testing machine. The data were recorded and analyzed using TRAPEZIUM-X analysis software (version 1.5.7, Shimadzu Corporation). Statistical analysis was performed using Welch's t-test to compare mechanical parameters (elastic modulus, compressive stress, hysteresis loss, and peak force) between WPU and WPU/PEDOT groups, accounting for potentially unequal variances. Results are expressed as mean ± standard deviation (SD), and 95% confidence intervals (CI) were calculated for the differences between means to assess the magnitude and consistency of the reinforcing effect. Statistical significance was set at $p < 0.05$.

2.7. Electrochemical Characterization

Cyclic voltammetry (CV) experiments were conducted in a conventional three-electrode cell with the sponges as the working electrode, AglAgCl/KCl (3 M) as the reference electrode, and a platinum wire as the counter electrode, all at room temperature. Experiments were conducted in DPBS at room temperature. Cyclic voltammetry assays were performed in the range of −0.2 V − + 0.8 V at a scan rate of 200 mV s^{-1}. The specific capacitance (C) was calculated from the integrated area of the CV curves using the following equation

$$C = \frac{\int idV}{2 \times \nu \times \Delta V}$$

where $\int idV$ is the integrated area of the CV curve, ν is the scan rate (0.1 V/s), and ΔV is the electrochemical potential window (1.0 V). The results were normalized by the projected geometric area (0.636 cm^2) and the total mass (50 mg) of the cylindrical scaffolds to obtain the areal and gravimetric capacitance, respectively. All experiments were replicated at least 3 times using independent samples. Electrochemical characterization was carried out using an Autolab PGSTAT302N controlled by the NOVA software.

Electrochemical impedance spectroscopy (EIS) measurements were performed using a conventional three-electrode cell and an Autolab PGSTAT302N potentiostat/galvanostat operating between the frequency range of 100,000 and 0.1 Hz and 10 mV of amplitude for the sinusoidal voltage. Experiments were performed at room temperature. Platinum wire was used as the counter-electrode and Ag/AgCl/KCl (3 M) was employed as the reference electrode. Complex impedance data were fitted to equivalent electrical circuits using a Nonlinear Least Squares (NLLS) algorithm within the NOVA software. The goodness-of-fit was evaluated through the χ^2 parameter and the relative error percentage for each individual circuit element.

2.8. Loading of CR(*N*Me)KA Peptide and In Vitro Drug Release Studies

900 mg of WPU-GSSG were dispersed in PEDOT/PSS Clevios PH 1000 at a concentration of 30% w/v by autoclaving. Subsequently, 6 mL of CR(*N*Me)EKA peptide solution (7.5 mg/mL) in PEDOT/PSS (Clevios PH 100) were added. The resulting mixture was then poured into cylindrical molds (9 mm in diameter), frozen at −80 °C and lyophilized to obtain the final sponge.

To determine the drug loading, before lyophilization, 100 μL of mixture were diluted to 1 mL with DPBS and injected into HPLC. The calibration curve was determined using standard solutions of CR(*N*Me)EKA peptide in DPBS in the range 2−0.001 mg/mL. Drug loading efficiency (DL_E%) and entrapment efficiency (EE%) were calculated by the following formula

$$DL_E\% = \frac{\text{weight of encapsulated peptide}}{\text{mass of WPU/PEDOT + peptide}} \times 100$$

$$EE\% = \frac{\text{weight of encapsulated peptide}}{\text{weight of total added peptide}} \times 100$$

Peptide release studies from sponges were carried out in an orbital shaker at 37 °C and 50 rpm. Specifically, the sponges (mean weight of 50 mg, 9 mm in diameter, 6 mm in height) were placed in 6 mL of DPBS at pH 7.4 without or with the addition of DTT 10 mM.

Electro stimulated release studies were performed by applying chronoamperometry (CA) cycles as the electrical stimulus. Experiments were carried out using an Autolab PGSTAT302N potentiostat controlled by NOVA software in a three-electrode configuration. The setup employed a platinum counter electrode, an AglAgCl reference electrode, and the sponge as the working electrode. The sponge was positioned between a stainless-steel support and a Transwell insert membrane (with the membrane removed). The release medium was 6 mL of DPBS at pH 7.4 without or with the addition of DTT 10 mM.

https://doi.org/10.1021/acsapm.6c00875
ACS Appl. Polym. Mater. 2026, 8, 8479−8494

CA cycles were applied for 2 h to stimulate the release from the sponge. Each cycle consisted of a potential step to +0.50 V for 100 s, followed by an open-circuit interval of 300 s. This sequence was then repeated (potential step at +0.50 V for 100 s, open circuit for 300 s) throughout the 2 h experiment. At each time point, medium was withdrawn and replaced. The collected medium was lyophilized, redispersed in 1 mL of distilled water and injected into HPLC detecting the amount of peptide released until 21 days. All experiments were performed in triplicate (n = 3).

For kinetic analysis, the cumulative release data were normalized to the total amount of peptide released at 21 days (M_∞), and the fractional release (M_t/M_∞) was calculated at each time point. The release kinetics were evaluated using the Korsmeyer−Peppas model ($M_t/M_\infty = Kt^n$) by applying a logarithmic linearization ($\log(M_t/M_\infty) = \log K + n\cdot\log t$). Only data points corresponding to Mt/M∞ < 0.6 were included in the fitting procedure. Linear regression of $\log(M_t/M\infty)$ versus $\log(t)$ was used to determine the kinetic exponent (n) and the release constant (K), with the goodness of fit assessed by the coefficient of determination (R^2).

2.9. Quantification of CR(*N*Me)EKA Peptide (HPLC)

CR(*N*Me)EKA was quantified using an ACQUITY Arc System from Waters Corporation at room temperature with UV detection at 220 nm, using an XBridge Premier Peptide BEH C18 (130 Å, 2.5 μm, 4.6 × 150 mm) column. The HPLC method was isocratic for 25 min at 0.5 mL/min with the mobile phase consisting of 10% acetonitrile, 10% methanol and 80% water, modified with 0.1% trifluoroacetic acid, and a 20 μL injection volume.

2.10. Cell Culture Assays

2.10.1. Cell Culture Maintenance. Cellular assays were performed using the human prostate cancer cell line (PC-3) and the human normal prostate cell line (PNT-2), which were cultured in Ham's F-12K (Kaighn's) medium and Roswell Park Memorial Institute (RPMI) medium, respectively. F-12K medium was supplemented with 10% fetal bovine serum (FBS) and 1% antibiotic solution (penicillin 100 units/mL, streptomycin 100 μg/mL). RPMI medium was supplemented with 1% L-glutamine (200 mM stock solution), and 1% antibiotic and antimycotic solution (penicillin 100 units/mL, streptomycin 100 μg/mL, and amphotericin 25 μg/mL). Cultures were maintained in a humidified incubator with an atmosphere of 5% CO_2 and 95% O_2 at 37 °C. Culture media were changed every 2 days. Cell passaging was performed in 1:3 split ratio. When the cells reached 80−90% confluence, they were detached using 1 mL of trypsin (0.25% trypsin/EDTA) for 3 min at 37 °C. Finally, cells were resuspended in 5 mL of fresh medium and their concentration was determined by staining with 0.4% trypan blue and counting was performed with an automatic cell counter Countess 3 (Thermo Fisher Scientific, USA), using an average of two counts.

2.10.2. In Vitro Cytocompatibility Studies. The tested sponges (WPU and WPU/PEDOT) were placed in 24-well plates and sterilized using UV irradiation for 30 min on each side, in a laminar flow hood. Then, cells were seeded on top of the sponges using the concentrated droplet method and allowed to infiltrate the sample for 30 min. After which, the appropriate medium was added to fully cover the samples. Controls were simultaneously performed by culturing the cells on the surface of the well.

For adhesion (1 day) and proliferation (7 days) assays, cells were seeded at a density of 2 × 10^4 cells/sample and 5 × 10^4 cells/sample, respectively, in 24-well plates for 24 h or 7 days in a humidified incubator with an atmosphere of 5% CO_2 and 95% O_2 at 37 °C. Cellular viability was evaluated by the colorimetric MTT [3-(4, 5-dimethylthiazol-2-yl)-2, 5-diphenyltetrazolium bromide] assay. Specifically, after discarding the medium, 1 mL of MTT solution (5 mg/mL in medium) was added to each well in the 24-well plates. After 3 h of incubation at 37 °C, medium was discarded and 1 mL of DMSO was added to each well to dissolve formazan crystals. Finally, the absorbance was measured in a plate reader at 570 mm. The viability results correspond to the average of three independent replicas (n = 3) for each system. Results were normalized to the control, for relative percentages.

2.10.3. Confocal Microscopy. For adhesion (1 day) and proliferation (7 days) assays, cells were seeded at a density of 2 × 10^4 cells/sample and 5 × 10^4 cells/sample, respectively, in 24-well plates for 24 h or 7 days in a humidified incubator with an atmosphere of 5% CO_2 and 95% O_2 at 37 °C. After the incubation period, cells were fixed using 2.5% glutaraldehyde solution in PBS, washed with PBS, and stained with Alexa Fluor 488 phalloidin for visualizing actin cytoskeleton and with Hoechst dye to visualize the nuclei. Samples were protected from light and kept at 4 °C before imaging, which was performed using a 10× objective of an Axio Observer 7 Confocal laser microscope (Carl ZEISS LSM 800, Germany). Image processing was completed with ZEN software (ZEISS, Germany), and ImageJ software (Wayne Rasband, NIH, USA).

2.10.4. In Vitro Electrostimulation Assays and Cytotoxicity Evaluation. The sponges (mean weight of 50 mg, 9 mm in diameter, 6 mm in height), which were placed in Transwell inserts, were sterilized using UV irradiation for 30 min in a laminar flow hood. For the ES procedure, the following setup was prepared: two stainless steel plates were used as electrodes in a two-electrode setup, with one plate attached to one side of a well of a 24-well plate and the other plate put in direct contact with the sponge that was placed inside a Transwell insert (as shown in Scheme 1). The stainless-steel plates were previously sterilized by UV light exposure for 30 min inside a laminar flow hood. Then, the PNT-2 cells and the PC-3 cells were seeded (1 × 10^5 cells/mL) in a 24-well plate and incubated at 37 °C and 5% CO_2 for 24 h. After this, media was replaced with fresh one, and the sponges and stainless-steel electrodes were attached to the plate. ES was performed using a two-electrode system, where the working electrode was connected to the sponge samples (WPU, WPU/PEDOT and WPU/PEDOT/CR(*N*Me)EKA) and the reference/counter electrode was in contact with the cell medium. A fixed voltage of +0.5 V was applied (fast chronoamperometry mode; Metrohm μStat-i 400s Potentiostat/Galvanostat/Impedance Analyzer) for 2 h. A second assay was performed in the same way, but incubating the cells with the samples for another 24 h (for both cell lines) and 4 days (for PNT-2 cells) to allow further release of the peptide. Nonelectro stimulated control sponges were also tested. Quantitative evaluation of the effect of ES on the cells was performed by the MTT assay, as described above. For visual qualitative cell viability assays following ES, the same procedure of ES was followed as described above. PC-3 cells were stained with calcein red-orange AM to visualize live cells with and without ES, using a 10× objective of an Axio Observer 7 Confocal laser microscope (Carl ZEISS LSM 800, Germany). Image processing was completed with ZEN software (ZEISS, Germany), and ImageJ software (Wayne Rasband, NIH, USA).

Scheme 1. Schematic Representation of the Setup used for In Vitro Electrostimulation (ES) Assays with PC-3 and PNT-2 Cells

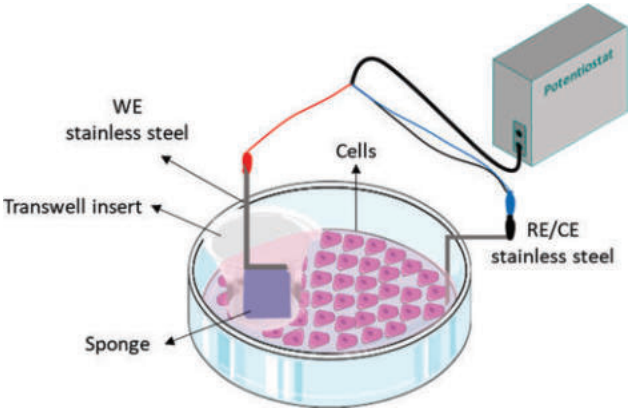

https://doi.org/10.1021/acsapm.6c00875
ACS Appl. Polym. Mater. 2026, 8, 8479−8494

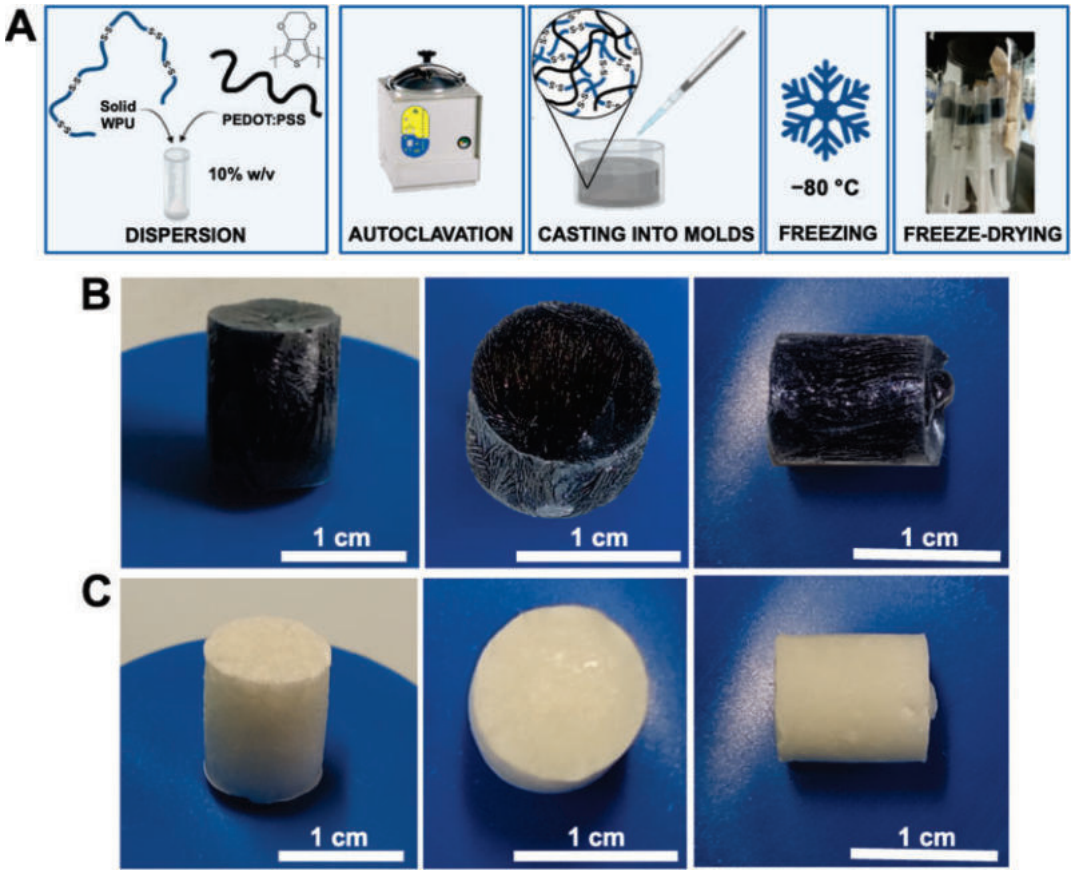

Figure 1. Schematic representation of the production procedure and representative images of sponges. (A) Schematic illustration of the production process for WPU/PEDOT sponges. (B) Images of WPU/PEDOT sponges showing the characteristic dark-blue coloration imparted by the conductive PEDOT phase, indicative of successful polymer incorporation and homogeneous dispersion. (C) Images of corresponding WPU sponges without PEDOT, displaying their typical light, whitish appearance.

2.11. Statistical Analysis

Statistical analyses were performed using GraphPad Prism v9.0. All quantitative data are expressed as mean ± standard deviation (SD) of at least three independent experiments (n = 3 for swelling, hydrolytic degradation, peptide release, and biological assays; n = 6 for mechanical testing). Statistical significance was determined using parametric tests depending on the data set characteristics. The structural divergence between pore size distributions (microCT analysis) was evaluated using the two-sample Kolmogorov−Smirnov test. For the comparison of mechanical properties between pristine and composite sponges, Welch's t-test was employed to account for potential unequal variances between formulations. For time-dependent experiments, including swelling behavior, hydrolytic degradation profiles, in vitro peptide release kinetics, and electrostimulation cytotoxicity assays, a two-way analysis of variance (two-way ANOVA) was performed. All ANOVA procedures were followed by Šídák's posthoc test for multiple comparisons to assess differences between specific groups. A probability value of $p < 0.05$ was considered statistically significant.

3. RESULTS AND DISCUSSION

3.1. Fabrication and Structural Characterization of WPU/PEDOT Sponges

Electroconductive porous sponges were successfully fabricated by dispersing WPU-GSSG[27] (10% w/v) within an aqueous PEDOT/PSS dispersion using an autoclave-assisted process (Figure 1A). This step ensured complete homogenization of the polymeric phases and promoted intimate interactions between the redox-responsive polyurethane matrix and the conductive PEDOT network. Subsequent freezing at −80 °C followed by lyophilization yielded lightweight, mechanically stable cylindrical sponges (Figure 1B). The WPU-to-PEDOT ratio was selected based on previous studies,[19−25] aiming to balance mechanical stability, electroactivity, and cytocompatibility. This ensures a continuous conductive network while maintaining scaffold robustness and safety. Nonconductive control sponges were prepared under identical conditions using distilled water instead of PEDOT/PSS (Figure 1C), resulting in reproducible architectures suitable for comparative analysis.

Microcomputed tomography (micro-CT) morphometric analysis was employed to quantitatively assess the impact of PEDOT/PSS incorporation on the internal architecture of the WPU scaffolds (Figure 2A). As summarized in Figure 2A, the introduction of the conductive filler induced a profound structural remodeling from a homogeneous cellular matrix to an anisotropic channeled network. WPU/PEDOT sponges exhibited a significantly higher total porosity (73.91%) compared to PEDOT-free WPU sponges (55.93%), a shift primarily driven by a 3-fold increase in mean structure separation (St.Sp), which rose from 20.93 ± 6.45 μm to 56.61 ± 29.29 μm. Statistical analysis of the pore size distribution (Figure 2A) further elucidates this transition: while WPU scaffolds displayed a narrow, Gaussian-like distribution (CV = 30.8%), the WPU/PEDOT system showed

https://doi.org/10.1021/acsapm.6c00875
ACS Appl. Polym. Mater. 2026, 8, 8479−8494

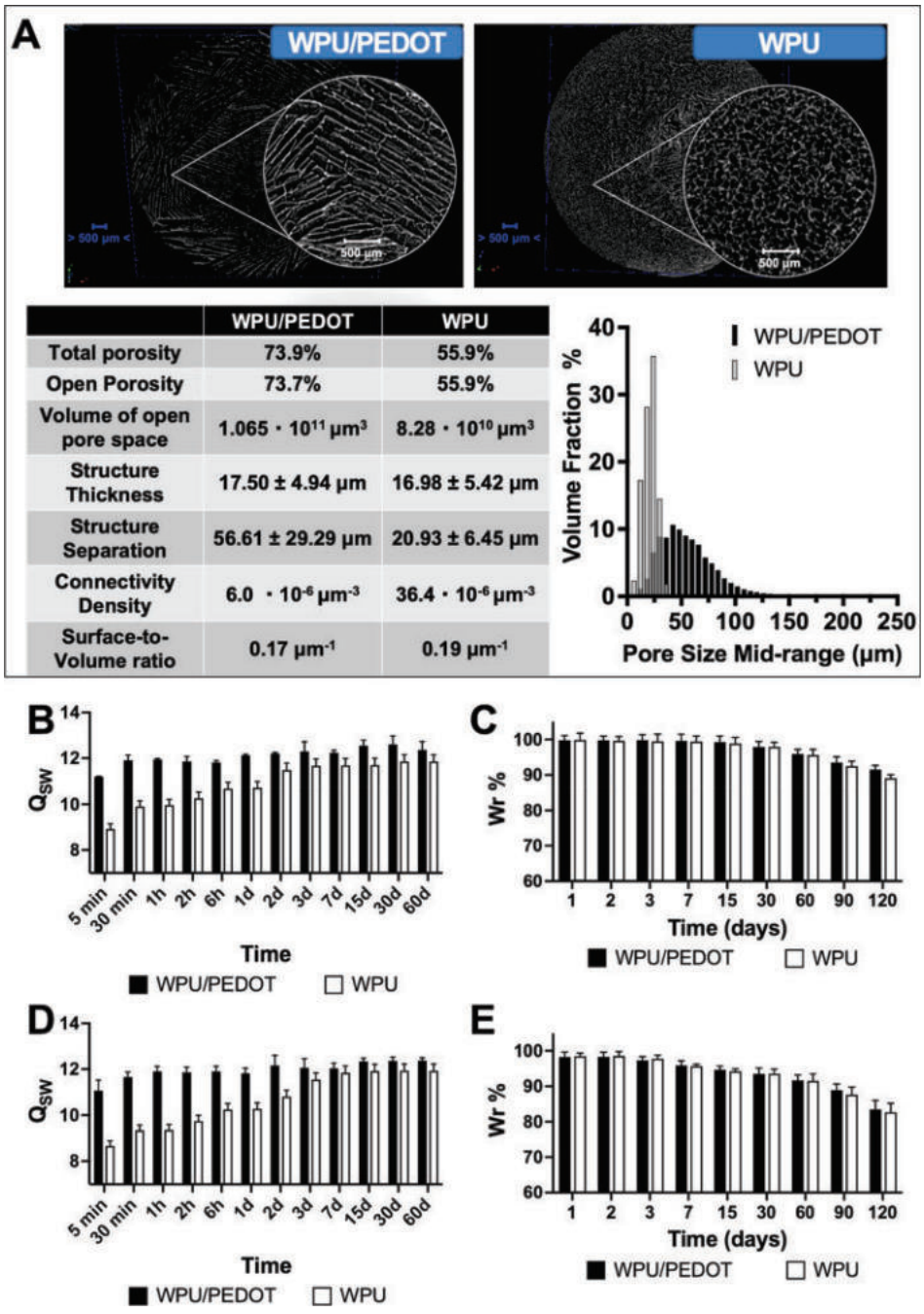

Figure 2. Morphometric characterization and functional properties of the sponges. (A) Representative 3D micro-CT reconstructions of WPU/PEDOT and WPU sponges, with circular insets highlighting the structural anisotropy induced by the conductive filler. The table summarizes key morphometric parameters: total porosity, open porosity, structure thickness (St.Th), and structure separation (St.Sp). The histogram displays the volumetric pore size distribution; the statistical divergence between the two populations was validated using the two-sample Kolmogorov−Smirnov test (D = 0.50, p < 0.001). (B) Swelling behavior in DPBS; (C) Hydrolytic degradation in DPBS; (D) Swelling behavior in simulated reductive environment (DPBS + 10 mM DTT); (E) hydrolytic degradation in simulated reductive environment (DPBS + 10 mM DTT).

a markedly heterogeneous and broadened profile (CV = 51.7%). The divergence between the two volumetric populations was statistically confirmed by a two-sample Kolmogorov−Smirnov test (D = 0.50, p < 0.001), reflecting a fundamental shift in the ice-templating kinetics. This structural divergence, occurring while the wall thickness remained nearly invariant (St.Th ≈ 17 μm), suggests that PEDOT/PSS acts specifically as a phase-modifier during the ice-templating process. We hypothesize that the polyelectrolyte nature of PEDOT/PSS alters the rheological properties and thermal conductivity of the precursor dispersion, hindering isotropic ice growth and favoring the formation of elongated, highly interconnected channels.[30,31] Such architectural features, corroborated by the open porosity (>99% of the total void fraction), are expected to significantly enhance the scaffold's permeability, facilitating fluid transport and molecular diffusion, which are critical for the observed drug release kinetics.

https://doi.org/10.1021/acsapm.6c00875
ACS Appl. Polym. Mater. 2026, 8, 8479−8494

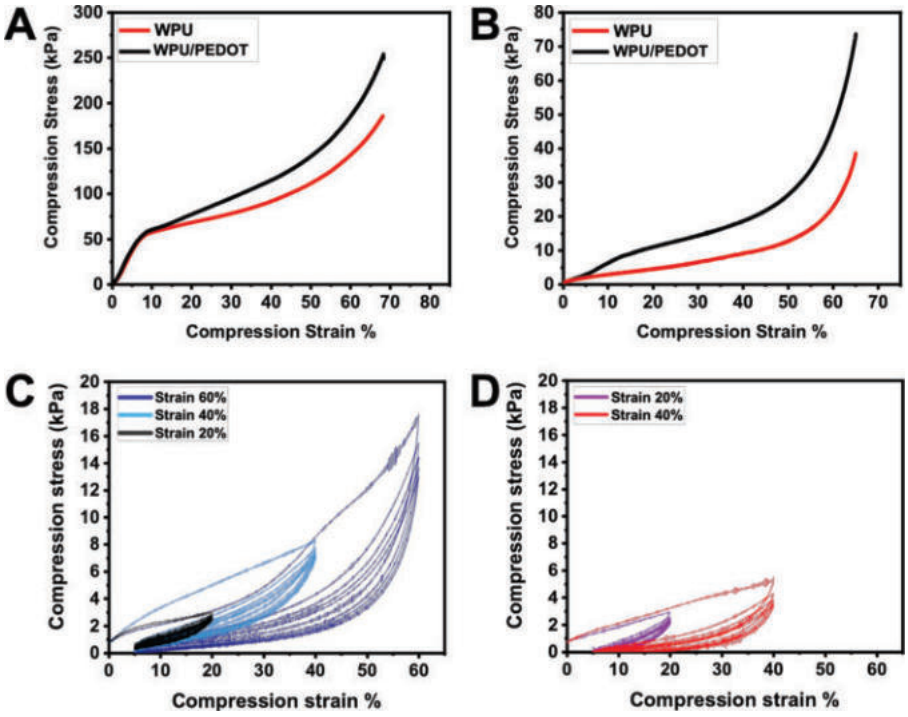

Figure 3. Mechanical characterization of WPU/PEDOT sponges. (A) Representative stress−strain curves in the dry state and (B) in the swollen state. Quantitative analysis (n = 6, mean ± SD) and statistical comparisons (Welch's t-test) are reported in the main text. (C) Cyclic compression tests in the swollen state for WPU/PEDOT (up to 60% strain) and (D) pristine WPU sponges (up to 40% strain). The absence of the 60% cycle for pristine WPU highlights its structural instability and failure at high deformation levels. Quantitative evaluation of hysteresis loss and peak compressive force is provided in the text.

Swelling studies conducted in DPBS at 37 °C highlighted pronounced differences between the two formulations (Figure 2B). WPU/PEDOT sponges rapidly absorbed aqueous media, reaching equilibrium swelling within approximately 30 min, whereas PEDOT-free WPU sponges required up to 3 days to attain comparable hydration levels. Two-way ANOVA confirmed a significant effect for both formulation and time (p < 0.0001). Posthoc analysis using Šídák's multiple comparisons test revealed a high statistical significance in the initial phase (5 min to 1 day, p < 0.0001), with a mean difference in swelling ratio of 2.27 already at 5 min (95% CI: 1.66−2.89). This accelerated uptake is consistent with the higher porosity and anisotropic, channeled pore morphology observed by micro-CT, which enables rapid liquid penetration throughout the scaffold. Such fast hydration is advantageous for implantable drug delivery systems, ensuring prompt activation after implantation and efficient initiation of drug diffusion.[32]

Long-term hydrolytic stability was evaluated over 120 days in DPBS (Figure 2C). Both WPU and WPU/PEDOT sponges retained approximately 85% of their initial mass after four months, indicating excellent resistance to hydrolytic degradation. Statistical analysis confirmed that the incorporation of PEDOT/PSS did not significantly alter the degradation profile (p > 0.99 for all time points), with a negligible mean difference between the two formulations at the end of the study (2.43%, 95% CI: −1.16−6.01, p = 0.3928). The gradual mass loss observed is consistent with slow ester bond cleavage within the soft segments of the WPU-GSSG backbone.

Notably, exposure to a reducing environment (DPBS containing 10 mM DTT) did not significantly alter either the swelling behavior or degradation profile of the sponges (Figure 2D,E). In the reductive medium, WPU/PEDOT maintained its significantly faster swelling kinetics (p < 0.0001 from 5 min to 2 days), while the degradation profile showed no significant divergence between the two groups (p > 0.96 at all intervals). As already reported, despite the reductive cleavage of disulfide bonds, the freeze-dried WPU-GSSG microstructure resists to rapid depolymerization under mild reducing conditions. This stability arises from the hydrophobic domains in the WPU, which form strong physical interactions that are not disrupted by GSSG reduction.[27] These findings indicate the suitability of WPU/PEDOT-based sponges for applications in implantable and stimuli-responsive systems where rapid hydration and sustained mechanical integrity are important functional requirements.

3.2. Mechanical Characterization

Compression testing revealed that PEDOT incorporation markedly influenced the mechanical response of the sponges under both static and cyclic loading. In the dry state (Figure 3A), WPU/PEDOT sponges exhibited a significantly higher elastic modulus (680 ± 77 kPa) compared to PEDOT-free WPU sponges (532 ± 58 kPa). The mechanical reinforcement provided by the PEDOT/PSS network was rigorously evaluated using Welch's t-test, which accounts for potential unequal variances between the composite formulations. The analysis confirmed a significant increase in the elastic modulus for WPU/PEDOT sponges compared to pristine WPU (t(7.38) = 4.02, p = 0.0045, n = 6). The 95% confidence interval (CI) for the difference between means ranged from 59.74 to 225.9 kPa, highlighting the consistency of the reinforcing effect. Similarly, the compressive stress at 60% strain was significantly enhanced upon PEDOT integration,

https://doi.org/10.1021/acsapm.6c00875
ACS Appl. Polym. Mater. 2026, 8, 8479−8494

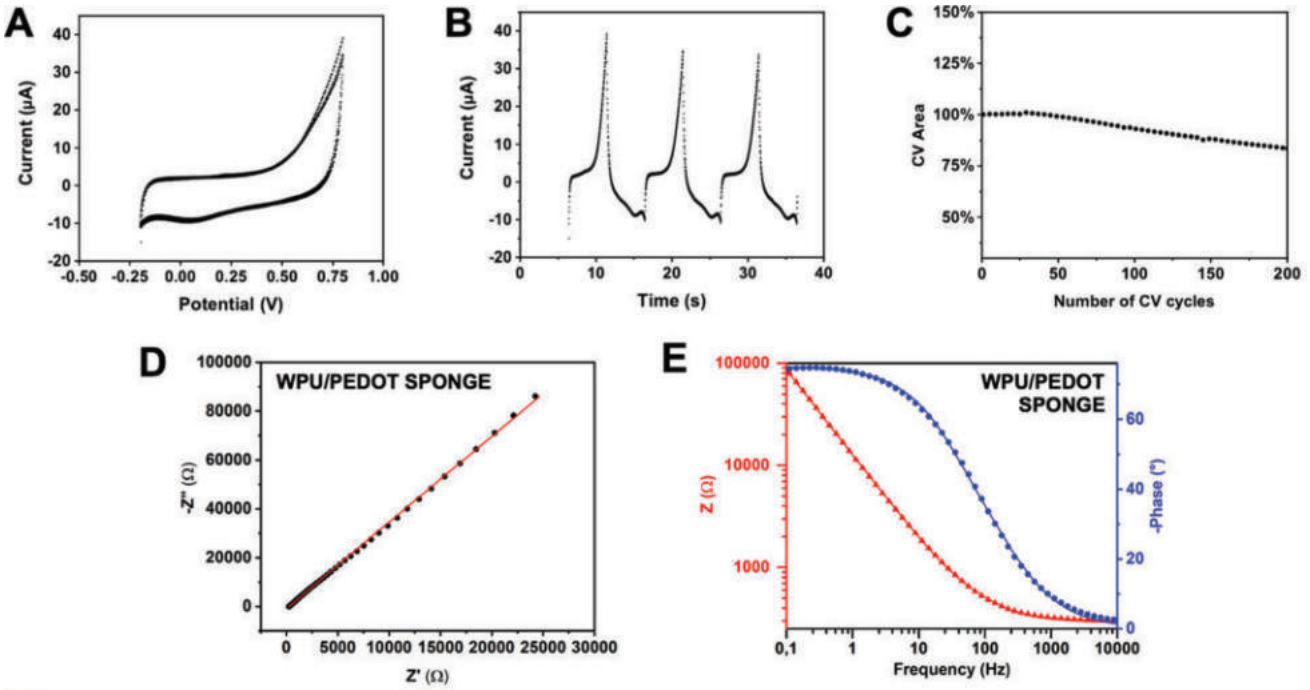

F

WPU/PEDOT SPONGE

Element	Parameter	Value	Relative Error %
R1	R	235 Ω	0.44
R2	R	860 Ω	4.80
Q1	Y0	15.2 μMho·s^n	4.49
	N	0.815	0.41
Q2	Y0	1.23 μMho·s^n	2.39
	N	0.936	4.93
Fit Metric	χ^2	0.073	

WPU SPONGE

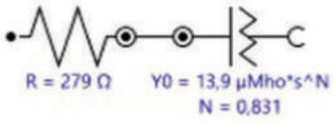

Element	Parameter	Value	Relative Error %
R1	R	279 Ω	0.34
Q1	Y0	13.9 μMho·s^n	0.48
	N	0.831	0.15
Fit Metric	χ^2	0.070	

Figure 4. Electrical characterization of WPU/PEDOT sponges: (A) CV showing current response as a function of applied voltage; (B) CV current response plotted over time; (C) stability assessment of the electrochemical performance, expressed as the percentage of CV integrated area for each cycle relative to the first cycle, over 200 consecutive CV scans; (D) EIS Nyquist plot, depicting real versus imaginary impedance components; (E) EIS presented as Bode plot, illustrating frequency-dependent impedance magnitude and phase; (F) equivalent electrical circuit model used to fit EIS data, including the associated fitting parameters and relative error percentages for each element.

increasing from 185.6 ± 25 kPa for WPU to 233.3 ± 22 kPa for WPU/PEDOT (Welch's *t*-test: $t(9.89) = 3.47$, $p = 0.0061$, $n = 6$, 95% CI: 17.01 to 78.47 kPa). These improvements arise from PEDOT/PSS acting as a rigid, percolating secondary phase within the elastomeric WPU-GSSG matrix, enhancing stress transfer and reinforcing the porous network.[33−35] The autoclave-assisted dispersion step ensures intimate mixing between PEDOT/PSS and WPU, favoring the formation of load-bearing microdomains that become particularly effective after the removal of water during lyophilization.[36]

After equilibration in DPBS for 24 h, both sponge types softened due to water uptake; however, WPU/PEDOT sponges retained superior mechanical performance (Figure 3B). Welch's *t*-test revealed a highly significant difference in

https://doi.org/10.1021/acsapm.6c00875
ACS Appl. Polym. Mater. 2026, 8, 8479−8494

the hydrated elastic modulus ($t(8.98) = 6.06$, $p = 0.0002$), with 40.5 ± 2.8 kPa for WPU/PEDOT compared to 28.2 ± 4.5 kPa for WPU (95% CI: 7.67 to 16.83 kPa). Consistently, the hydrated compressive stress at 60% strain also showed a significant increase, rising from 40.5 ± 1.1 kPa for WPU to 58.1 ± 9.1 kPa for WPU/PEDOT ($t(9.97) = 3.23$, $p = 0.0091$, 95% CI: 5.42 to 29.69 kPa). The proportionally greater reinforcement observed in the hydrated state suggests that PEDOT stabilizes pore walls and mitigates water-induced plasticization. Importantly, the modulus of the hydrated WPU/PEDOT sponge falls within the range reported for human prostate tissue (∼15−40 kPa),[37] indicating favorable mechanical compatibility with the target tissue and could minimize stiffness mismatch upon implantation.

Cyclic compression tests further highlighted the enhanced resilience imparted by PEDOT (Figure 3C,D). WPU/PEDOT sponges exhibited complete elastic recovery (100%) at 20%, 40%, and 60% strain, whereas WPU sponges displayed residual deformation at 40% strain (96% recovery) and structural failure at 60%. Quantitative analysis of the hysteresis loops at 40% strain revealed that PEDOT incorporation significantly reduced energy dissipation (hysteresis loss) from 48.9 ± 5.2% for WPU to 38.5 ± 6.1% for WPU/PEDOT (Welch's t-test: $t(9.62) = 3.60$, $p = 0.0052$, $n = 6$). This represents a ∼21% improvement in elastic efficiency, with a 95% confidence interval for the difference ranging from 3.93% to 16.87%. Reduced hysteresis implies greater elastic efficiency and less structural rearrangement or internal friction during loading−unloading, features typically associated with more robust polymer networks or enhanced physical cross-linking.

Peak compressive force (F_{max}) measurements supported these findings. At 20% and 40% strain, WPU/PEDOT sponges showed an upward trend in load-bearing capacity, reaching 0.22 ± 0.07 N and 0.43 ± 0.11 N, respectively, compared to 0.18 ± 0.03 N and 0.36 ± 0.10 N for WPU. While the high variance within the composite group precluded statistical significance at low strains, a major divergence was observed at 60% strain. At this stage, WPU/PEDOT withstood forces up to 0.82 ± 0.15 N, whereas pristine WPU sponges underwent structural fracture and were unable to maintain consistent load-bearing. This confirms that the PEDOT/PSS network provides a critical reinforcing contribution that becomes deterministic under high-deformation conditions.

Together, these mechanical data indicate that PEDOT incorporation affects not only stiffness but also the cyclic durability and energy management of the sponge matrix. The improved performance under hydrated and dynamic conditions is particularly relevant for biomaterials intended for implantation in mechanically active environments, where structures may experience continuous deformation due to respiration, muscle movement, tissue compression, or pulsatile flow. Under such conditions, the ability to sustain repetitive loading without permanent deformation is essential for maintaining both structural integrity and consistent drug release performance over time.[38]

3.3. Electrochemical Characterization

The electrochemical behavior of WPU/PEDOT sponges was evaluated using cyclic voltammetry (CV) and electrochemical impedance spectroscopy (EIS). CV profiles (Figure 4A,B) exhibited well-defined anodic and cathodic peaks characteristic of reversible PEDOT redox processes,[39] confirming that electroactivity was preserved after autoclaving and freeze-drying. Quantitative analysis of the CV integrated area (30.33 ± 1.25 μA·V, $n = 3$) yielded a specific areal capacitance of 0.238 ± 0.009 mF/cm^2 (corresponding to a gravimetric capacitance of 3.03 ± 0.13 mF/g and to a volumetric capacitance of 0.397 ± 0.016 mF/cm^3). These values fall within the expected range reported for PEDOT-based porous and hydrogel-like bioelectronic scaffolds, which typically exhibit sub-mF/cm^2 to mF/cm^2 areal capacitance depending on morphology, ionic accessibility, and percolation pathways.[40,41] This indicates that the microchanneled architecture effectively supports charge storage and distribution. Stability tests over 200 consecutive CV cycles showed only a ∼15% decrease in integrated charge (Figure 4C), confirming minimal degradation, low loss of electroactivity, and highlighting the robustness of the hybrid system under repeated electrochemical stress, indicating good electrochemical durability under repeated stimulation.

EIS measurements provided additional insight into charge transport and interfacial complexity. Nyquist plots (Figure 4D) revealed a lower total resistance for WPU/PEDOT sponges (235 Ω) compared to WPU sponges (279 Ω), indicating improved electrical conductivity upon PEDOT incorporation. The additional resistive element ($R_2 \approx 860$ Ω) observed in PEDOT-containing samples likely arises from interfaces between conductive and insulating domains within the porous network. Bode plots (Figure 4E) further supported these observations, showing differences in both impedance magnitude and phase angle, consistent with a more heterogeneous electrochemical environment. Such distributed responses are typical of porous systems, where ion transport and interfacial processes contribute to nonideal impedance behavior.[42] Equivalent circuit fitting (Figure 4F) confirmed the presence of multiple electrochemically distinct regions. The reliability of the fitting was validated by low relative errors for individual circuit elements (consistently <5%) and a X^2 value of 0.073, indicating a solid agreement between the model and the experimental data for these complex 3D architectures (see Figure 4F for detailed metrics). The WPU-only sponge could be modeled with a single Randles circuit (RC) element (Q), whereas the WPU/PEDOT sponge required two parallel RC branches ($Q1$ and $R^2\|Q^2$), indicative of multiple electrochemically distinct regions or interfaces introduced by PEDOT incorporation, as commonly observed in heterogeneous porous electrodes.[31] The total admittance (Y_0) increased from 13.9 to 16.43 μMho·s^n, and a higher constant phase exponent (n, from 0.831 to 0.936) was also observed, indicative of more ideal capacitive behavior and improved charge distribution upon PEDOT addition to the sponge structure, consistent with values typically reported for PEDOT-based and porous electrochemical systems.[43,44] This enhanced charge distribution is consistent with the anisotropic microchanneled morphology previously identified by micro-CT.

These findings demonstrate that PEDOT integration enhances the electrical properties of WPU sponges by introducing a multiphase conductive network that improves charge transport and distribution while maintaining electrochemical stability under repeated cycling. The combination of preserved redox activity, reduced resistance, increased admittance, and a more ideal capacitive behavior suggests that the WPU/PEDOT sponges are well-suited for electrically responsive applications, including stimuli-triggered drug release, biosensing, or local electrostimulation in implantable systems.[45]

https://doi.org/10.1021/acsapm.6c00875
ACS Appl. Polym. Mater. 2026, 8, 8479−8494

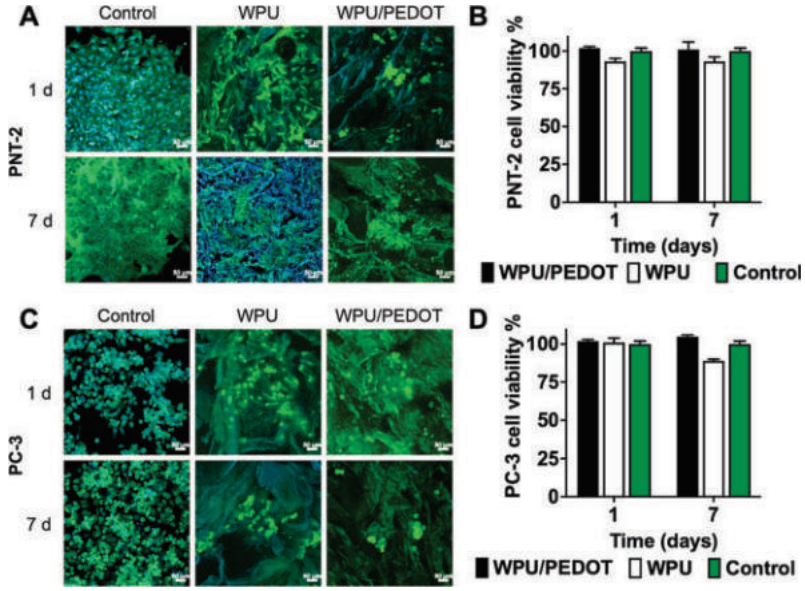

Figure 5. Cytocompatibility evaluation of the sponges with PNT-2 and PC-3 cells. (A) Confocal microscopy image of PNT-2 cells showing widespread distribution of viable cells with preserved morphology; (B) quantitative analysis of PNT-2 cell viability compared to the control, confirming high survival rates and absence of cytotoxic effects; (C) confocal microscopy image of PC-3 cells highlighting homogeneous colonization and viability; (D) quantitative analysis of PC-3 cell viability compared to the control, demonstrating consistently elevated values and confirming the cytocompatibility of the sponges.

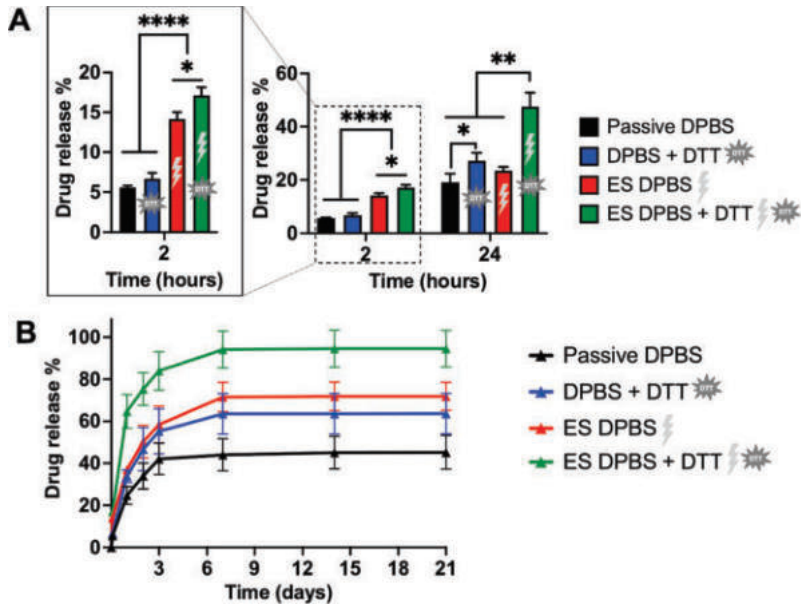

Figure 6. CR(*N*Me)EKA peptide release studies from WPU/PEDOT sponges: comparison of drug released in normal environment, in simulated reducing environment (10 mM DTT), in the presence of electrical stimulation and in the presence of both reducing and electrical stimulations (A) after 2 h and in the next 24 h; (B) cumulative drug release. Data are presented as mean ± SD ($n = 3$). Statistical differences were determined by two-way ANOVA followed by Šidák's multiple comparisons test. Symbols: *$p < 0.05$, **$p < 0.01$, ****$p < 0.0001$.

3.4. Cytocompatibility Studies

Assessment of cytocompatibility represents a critical step in the evaluation of novel biomaterials for biomedical applications, particularly for porous scaffolds designed to support cell adhesion, proliferation, and three-dimensional tissue integration. In this study, WPU and WPU/PEDOT sponges were tested using two representative prostate cell lines: PNT-2, an immortalized normal epithelial line, and PC-3, a highly metastatic prostate cancer line, providing insight into scaffold performance in both healthy and pathological cellular environments.

Confocal microscopy analysis (Figure 5A,C) revealed that cells readily adhered to the surface of both types of sponges and established intimate contact with the internal porous architecture, resulting in a widespread and homogeneous cell distribution. Actin staining with Alexa Fluor 488 phalloidin demonstrated well-organized cytoskeletal structures, while Hoechst staining confirmed intact and clearly defined nuclei. These observations indicate preservation of normal cellular

https://doi.org/10.1021/acsapm.6c00875
ACS Appl. Polym. Mater. 2026, 8, 8479−8494

morphology and the absence of cytotoxic effects. The interconnected pores and high porosity of the sponges likely facilitated nutrient and oxygen diffusion, promoting sustained cell survival within the 3D scaffold.[46,47]

Quantitative evaluation of cell viability via MTT assay (Figure 5B,D) supported these qualitative findings. Both PNT-2 and PC-3 cells exhibited consistently high viability after 1 day (adhesion) and 7 days (proliferation) of culture on WPU and WPU/PEDOT sponges, with values comparable to the cellular control grown in a non-3D environment. No significant differences were observed between the PEDOT-containing and PEDOT-free sponges, suggesting that the incorporation of PEDOT does not adversely affect cytocompatibility, despite its conductive nature. This is consistent with the chemical stability of PEDOT within the scaffold matrix and the absence of leachable toxic byproducts following autoclaving and lyophilization.

Overall, these studies demonstrate that prostate cells maintain optimal viability even when in direct contact with the material, indicating a high degree of cytocompatibility and supporting the safety of the system for interaction with the tissues in which it is intended to be implanted. The adoption of a three-dimensional culture configuration is therefore used as an in vitro model to more realistically reproduce cell-material contact and spatial constraints encountered in vivo. In this context, the preserved viability and morphology of both normal and cancerous prostate cells further validate the relevance of this 3D platform for assessing the biological safety and performance of localized drug delivery systems.

3.5. In Vitro CR(*N*Me)EKA Peptide Release Studies

To evaluate the capability of WPU/PEDOT sponges to encapsulate and release bioactive molecules, we selected the highly hydrophilic pentapeptide CR(*N*Me)EKA (Cys-Arg-*N*-methyl-Glu-Lys-Ala), an engineered analog of CREKA (Cys-Arg-Glu-Lys-Ala).[26,48,49] CREKA and its analogs interact with fibrin-fibronectin complexes in tumor vasculature, promoting accumulation at the tumor periphery and enhancing retention of therapeutic agents.[23,50] CR(*N*Me)EKA demonstrated significant anticancer efficacy, including induction of prostate tumor necrosis and reduction of tumor growth.[43] Its high hydrophilicity and bioactivity make CR(*N*Me)EKA an ideal candidate to investigate peptide loading, retention, and stimuli-responsive release from the hybrid WPU/PEDOT sponges.

The peptide was homogeneously incorporated into the WPU/PEDOT sponges during fabrication, achieving a drug loading of 4.5 ± 0.2% w/w and an entrapment efficiency of 99.5 ± 0.3% (n = 4). Under physiological conditions, passive release was limited (~5.6 ± 0.2% after 2 h), whereas exposure to reducing conditions slightly accelerated release (~6.7 ± 0.7%) (Figure 6A, n = 3). DTT was employed here as a stable and widely accepted surrogate for the reductive tumor microenvironment (TME). Although glutathione (GSH) is the primary endogenous reductant, DTT offers superior stability against auto-oxidation in aerobic conditions, providing a more reproducible model for validating the redox-triggered release mechanism.[51−55] This approach enabled clear isolation of the material's responsiveness to reductive stimuli as a proof-of-concept.

Application of electrical stimulation through chronoamperometry significantly enhanced release: after 2 h of potential cycling (+0.50 V for 100 s, open circuit 300 s), peptide release increased to 14.2 ± 0.8% in DPBS and 17.1 ± 1.0% in DPBS + DTT (n = 3, $p < 0.0001$ compared to passive control), highlighting the capacity of the PEDOT network to actively modulate peptide release. Extending the observation to 24 h (Figure 6A), passive release reached 19.1% in DPBS and 27.1 ± 2.9% with DTT, whereas electrically stimulated sponges released 23.5 ± 1.4% in DPBS and 47.6 ± 5.1% in DPBS + DTT. These results demonstrate the additive and synergistic effect of dual stimuli, with a statistically significant difference between the combined stimulation and single-stimulus groups (Two-way ANOVA, $p < 0.01$). In our previous studies, we demonstrated that under reductive simulated conditions, the GSSG moieties within the WPU were reduced to GSH.[27,29,56] In the present work, this redox-responsive behavior of WPU facilitates peptide release, confirming that modulation of the GSSG/GSH redox couple integrated into the polyurethane backbone promotes peptide release without compromising the overall structural stability of the sponge (see hydrolytic stability studies). In parallel, electrical stimulation further enhances peptide mobilization and diffusion from the scaffold. A positive bias of +0.5 V was applied to the system, inducing oxidation of PEDOT. This oxidation increases the density of charge carriers within the polymer, promoting the expulsion of positively charged ions from its matrix. Concurrently, the polymer undergoes a conformational transition from the benzoid to the quinoid structure. This structural rearrangement typically leads to a reduction in polymer volume, as the polymer chains contract, thereby facilitating the release of the peptide from the matrix.[57−60] Cumulative release over 7 days (Figure 6B) shows clearly the dual responsiveness of the system. Peptide release reached 44.0 ± 7.6% in DPBS, 63.6 ± 9.7% in DPBS + DTT, 71.5 ± 6.9% under electrical stimulation alone, and up to 94.1 ± 8.9% when electrical stimulation was combined with DTT. Pairwise comparisons using Šídák's multiple comparisons test indicated that the synergistic effect of the dual stimuli (electrical stimulation + DTT) was statistically significant compared to all individual conditions ($p < 0.01$).

To provide a deeper quantitative insight into the release physics, the cumulative data up to 60% of the total release were fitted using the Korsmeyer-Peppas model ($M_t/M_\infty = Kt^n$). The fitting revealed consistently low n values across all experimental conditions ($n \approx 0.28$ for DPBS, 0.32 for DPBS + DTT, 0.19 under electrical stimulation, and 0.23 under combined stimulation), indicating that peptide release from the porous WPU/PEDOT sponge is predominantly governed by diffusion-assisted transport within the hydrated porous network rather than by anomalous or relaxation-controlled mechanisms. In contrast, the kinetic constant K progressively increased from passive (0.49) to stimulated conditions, reaching the highest values under electrical stimulation (0.72) and dual-stimuli conditions (0.91), thus confirming that both redox conditions and electro-responsive activation mainly act by accelerating transport kinetics rather than altering the fundamental diffusion-dominated mechanism.

The structural integrity of the CR(*N*Me)KA peptide postrelease was assessed via LC−MS analysis (Figure S1). Chromatographic profiles (HPLC and TIC) show a consistent elution peak at ≈3.3 min across all release conditions, indicating the absence of significant detectable degradation products. Mass spectra concurrently display the characteristic signals associated with the monomeric (≈249 m/z) and dimeric (≈521 m/z) peptide forms. These results are consistent with the preservation of the peptide's primary

https://doi.org/10.1021/acsapm.6c00875
ACS Appl. Polym. Mater. 2026, 8, 8479−8494

structure under the investigated release conditions, including the application of electrical stimulation.

The results highlight the complementary roles of WPU and PEDOT: the redox-responsive disulfide bonds in WPU promote peptide release under reducing conditions typical of the TME, and the conductive PEDOT network allows precise temporal control through externally applied electrical stimuli. The synergistic stimulation by a reductive microenvironment combined with external electrical stimulation weakens the strong interactions binding the CR(*N*Me)EKA peptide to the WPU/PEDOT sponge, thereby enabling its complete release.[61] This synergy is particularly advantageous in localized postsurgical therapy, enabling on-demand peptide delivery to residual tumor cells while minimizing systemic exposure.

In summary, the WPU/PEDOT sponges exhibit high peptide loading, redox-sensitive release, and electro responsiveness, establishing them as a versatile platform for smart, dual-stimuli-responsive drug delivery. The ability to combine endogenous (TME) and exogenous (electrical) triggers offers a powerful strategy to achieve controlled, on-demand therapeutic dosing, optimizing efficacy while reducing off-target effects.

3.6. In Vitro Electrostimulation Assays and Cytotoxicity Evaluation

The influence of electrostimulation (ES) on normal prostate cells and on prostate cancer cells viability was evaluated in the presence of the engineered conductive sponges, as shown in Scheme 1.[24] A constant potential of +0.5 V was applied for 2 h under fast chronoamperometry conditions, followed either by immediate MTT quantification or by an additional 24 h incubation period to assess delayed effects associated with electrically stimulated peptide release. Nonstimulated samples served as internal controls for each formulation. Statistical differences were determined by two-way ANOVA followed by Šídák's multiple comparisons test. Results are reported in Figure 7.

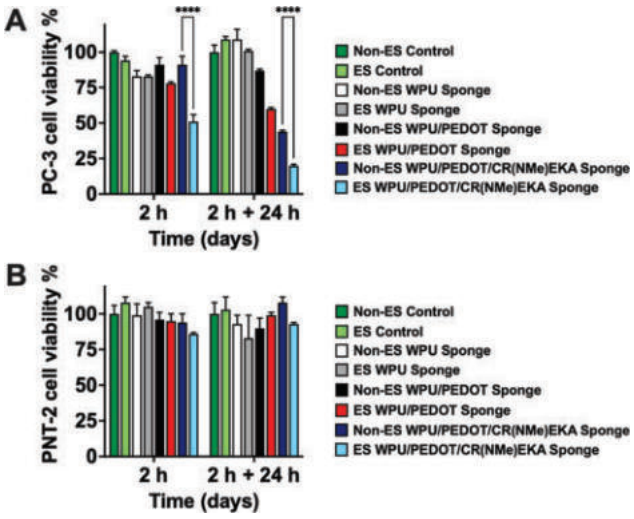

Figure 7. In vitro electrostimulation (ES) assays showing the cytotoxic effects of the sponges on (A) PC-3 cells and (B) PNT-2 cells, evaluated after 2 h of ES and after 2 h of ES followed by an additional 24 h of incubation. Data are expressed as mean ± SD (n = 3). Statistical significance was determined by two-way ANOVA followed by Šídák's multiple comparisons test (*p < 0.05, **p < 0.01, ***p < 0.001, **p < 0.0001).

As expected, WPU sponges, stimulated or not, preserved cell viability at levels comparable to untreated controls (ns, p > 0.05), confirming the intrinsic cytocompatibility of the redox-responsive polyurethane platform. Importantly, the ES protocol itself did not induce cytotoxicity: PC-3 cells maintained full viability after the 2 h stimulation, and a slight increase in metabolic activity was observed after 24 h (Figure 7A). This proliferative trend aligns with literature reporting that low-voltage electrical cues can transiently boost mitochondrial respiration and glucose uptake in certain cancer cell lines, likely via mild bioelectrical modulation rather than direct membrane disruption.[62,63] Furthermore, the +0.5 V chronoamperometric stimulus was selected as a proof-of-concept electrical activation parameter capable of stimulating the PEDOT/PSS conductive network while minimizing excessive electrochemical degradation. This voltage range was also supported by previous in vitro electrostimulation studies conducted by our group in the context of wound healing applications, where similar stimulation conditions demonstrated promising safety and biocompatibility profiles.[21,24]

To further verify that the applied ES conditions and the sponge materials did not elicit nonspecific toxicity, the same assays were conducted on normal prostate epithelial cells (PNT-2) (Figure 7B). Consistently, PNT-2 cells maintained high viability in both stimulated and nonstimulated controls, confirming that the ES protocol is intrinsically well tolerated by healthy cells (ns, p > 0.05). WPU sponges, without ES, preserved PNT-2 metabolic activity at ∼90−100%, indicating that the hybrid matrices are intrinsically cytocompatible. Even when ES was applied, only modest fluctuations in viability were observed, with values remaining >85% across all formulations. Cytocompatibility was further assessed up to 4 days after ES in PNT-2 cells (Figure S2), again with values near 100% (ns, p > 0.05). These results demonstrate that the materials and the electrical input do not compromise the viability of normal cells, providing an essential safety validation and confirming that the cytotoxic effects seen in PC-3 cells are not due to nonspecific material- or stimulation-dependent stress.

Incorporation of PEDOT into the polymer matrix significantly altered the cellular response under ES in the cancer model. In the absence of electrical input, WPU/PEDOT sponges induced only a modest reduction in metabolic activity in PC-3 cells, indicating limited basal interaction with the cells and confirming that the conductive polymer itself does not elicit overt toxicity when confined within the matrix. However, upon application of ES, PC-3 viability markedly decreased (∼60% after 24 h, p < 0.0001 vs nonstimulated control), suggesting that the conductive interface supports localized electrochemical reactions capable of perturbing cancer cell homeostasis. Possible mechanisms include modulation of extracellular redox conditions, generation of transient ionic gradients at the sponge−medium interface, and electrically enhanced adsorption or release of charged biomolecules.[64] Importantly, none of these effects were observed in PNT-2 cells under the same conditions (ns, p > 0.05 vs control), supporting a degree of tumor selectivity likely arising from intrinsic differences in electrical sensitivity, redox balance, differences in intrinsic cell membrane potential values and stress adaptation between normal and malignant cells.[65,66]

The strongest antitumor effect was observed for the peptide-loaded conductive sponges (WPU/PEDOT/CR(*N*Me)EKA). In the absence of ES, these scaffolds already induced a

https://doi.org/10.1021/acsapm.6c00875
ACS Appl. Polym. Mater. 2026, 8, 8479−8494

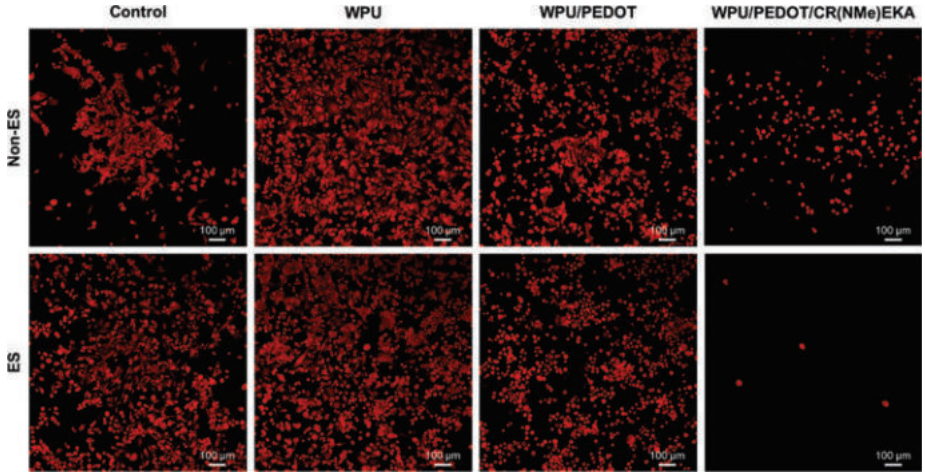

Figure 8. In vitro electrostimulation (ES) assays showing the cytotoxic effects of the sponges on PC-3 cells, evaluated after 2 h of ES followed by an additional 24 h of incubation. Calcein red-orange stained live cells.

significant decrease in PC-3 viability compared to the WPU control ($p < 0.01$), consistent with the pro-apoptotic activity of the CRE(*N*Me)EKA peptide and with its effective loading into the matrix (4.5 ± 0.2%). When ES was applied, PC-3 viability dropped dramatically, reaching values around ∼20% at 24 h ($p < 0.0001$ vs all other groups). This result was further observed by staining live PC-3 cells with calcein red-orange 24 h after ES was performed (Figure 8). It is possible to observe the decrease in live cell amount with the exposure to the WPU/PEDOT/CR(*N*Me)EKA sponge, being particularly accentuated in the presence of ES. Furthermore, cell morphology is also altered with the peptide presence, with cells losing their mostly elongated morphology and becoming rounder in shape. This pronounced effect strongly supports a synergistic interplay between PEDOT-mediated electrostimulation and peptide release. The electrical input likely accelerates peptide liberation by promoting electro-driven diffusion through the conductive network and by facilitating interactions with the cell membrane, thereby amplifying CR(*N*Me)EKA-dependent cytotoxic signaling, without its bioactivity being diminished by the loading and release processes.[23] Notably, this strong synergy was not mirrored in PNT-2 cells, which maintained high metabolic activity under both nonstimulated and ES conditions, indicating that the combined electrochemical insult is far more detrimental to cancer cells than to their healthy counterparts. The fact that this enhancement is achieved with a relatively low applied potential further underscores the efficiency and selectivity of the conductive−redox-responsive hybrid system.

Overall, these findings demonstrate that the WPU matrix provides an excellent cytocompatible foundation, while the integration of PEDOT enables precise electrical modulation of cellular responses. When combined with a therapeutic peptide, the resulting WPU/PEDOT/CR(*N*Me)EKA peptide sponge functions as a highly effective electro-chemotherapeutic platform capable of inducing potent, spatially confined cytotoxicity. The inclusion of PNT-2 data strengthens these conclusions by confirming that both the materials and the ES protocol are well tolerated by normal cells, and that the observed cytotoxicity in PC-3 cells arises from selective, cancer-specific mechanisms. This dual-responsive behavior substantiates the potential of conductive sponges and hydrogels for precision locoregional cancer therapy, where on-demand modulation of drug release and therapeutic activity can be externally controlled in real time while preserving the integrity of surrounding healthy tissues.

4. CONCLUSIONS

In this work, we developed and extensively characterized a multiresponsive porous sponge based on a glutathione-extended WPU integrated with PEDOT/PSS, designed for localized and on-demand anticancer peptide delivery. The combination of an autoclave-assisted dispersion process with freeze-drying enabled the fabrication of highly porous, mechanically robust sponges with interconnected micro-architectures. Incorporation of PEDOT/PSS significantly increased porosity, accelerated hydration kinetics, and enhanced mechanical performance under both static and cyclic compression, while maintaining modulus values within the range of native prostate tissue in the hydrated state. Thus, being compatible with implantation within native tissue.

Electrochemical analysis confirmed that the conductive network retained reversible PEDOT redox behavior and good cyclic stability after processing, supporting repeated electrical stimulation without substantial loss of electroactivity. Importantly, the integration of PEDOT introduced a stable electroconductive architecture capable of modulating interfacial charge transport and enabling electrically triggered functionality within the porous scaffold.

The sponges demonstrated excellent cytocompatibility toward normal prostate epithelial cells and supported three-dimensional cell adhesion and infiltration. When loaded with the tumor-homing peptide CR(*N*Me)EKA, the system exhibited minimal passive release and a pronounced dual-stimuli-responsive peptide release. Electrical stimulation and reductive conditions independently enhanced peptide release, while their combination produced a synergistic effect, enabling near-complete release over extended periods. This controlled release translated into selective cytotoxic effects against prostate cancer cells, particularly under ES, while preserving the viability of healthy cells.

Overall, this study establishes WPU/PEDOT/CR(*N*Me)-EKA sponges as mechanically compliant, electrochemically stable, and biologically selective platforms for electro-chemotherapeutic applications. By integrating redox responsiveness, electrical triggers, and peptide delivery within a single porous

https://doi.org/10.1021/acsapm.6c00875
ACS Appl. Polym. Mater. 2026, 8, 8479−8494

architecture, these systems expand the design space for implantable and locoregional cancer therapies. The modularity of the WPU chemistry and the versatility of the fabrication approach further suggest that this platform can be adapted to other therapeutic agents, stimulation modalities, and tissue targets.

■ ASSOCIATED CONTENT

Data Availability Statement

Data will be made available upon request.

Supporting Information

The Supporting Information is available free of charge at https://pubs.acs.org/doi/10.1021/acsapm.6c00875.

LC−MS analysis of the CR(NMe)KA peptide released under different conditions. In vitro electrostimulation (ES) assays showing the cytotoxic effects of the sponges on PNT-2 cells, evaluated after 2 h of ES followed by an additional 4 days of incubation (PDF)

■ AUTHOR INFORMATION

Corresponding Author

Leonor Resina − *IMEM-BRT Group, Departament d'Enginyeria Química, Escola d'Enginyeria de Barcelona Est (EEBE), Universitat Politècnica de Catalunya—BarcelonaTech (UPC), Barcelona 08019, Spain; Barcelona Research Centre in Multiscale Science and Engineering, Universitat Politècnica de Catalunya—BarcelonaTech (UPC), Barcelona 08019, Spain;* orcid.org/0000-0003-4216-8349; Email: maria.leonor.matos@upc.edu

Authors

Francesco Cancilla − *Dipartimento di Scienze e Tecnologie Biologiche Chimiche e Farmaceutiche (STEBICEF), Università degli Studi di Palermo, Palermo 90123, Italy;* orcid.org/0000-0002-8453-0804

Fabio Salvatore Palumbo − *Dipartimento di Scienze e Tecnologie Biologiche Chimiche e Farmaceutiche (STEBICEF), Università degli Studi di Palermo, Palermo 90123, Italy; Istituto per la Ricerca e l'Innovazione Biomedica (IRIB), CNR, Palermo 90146, Italy;* orcid.org/0000-0001-6196-7782

Calogero Fiorica − *Dipartimento di Scienze e Tecnologie Biologiche Chimiche e Farmaceutiche (STEBICEF), Università degli Studi di Palermo, Palermo 90123, Italy;* orcid.org/0000-0002-5169-4036

Giovanna Pitarresi − *Dipartimento di Scienze e Tecnologie Biologiche Chimiche e Farmaceutiche (STEBICEF), Università degli Studi di Palermo, Palermo 90123, Italy;* orcid.org/0000-0002-0815-9142

Maria M. Pérez-Madrigal − *IMEM-BRT Group, Departament d'Enginyeria Química, Escola d'Enginyeria de Barcelona Est (EEBE), Universitat Politècnica de Catalunya—BarcelonaTech (UPC), Barcelona 08019, Spain; Barcelona Research Centre in Multiscale Science and Engineering, Universitat Politècnica de Catalunya—BarcelonaTech (UPC), Barcelona 08019, Spain;* orcid.org/0000-0002-2498-8485

Carlos Alemán − *IMEM-BRT Group, Departament d'Enginyeria Química, Escola d'Enginyeria de Barcelona Est (EEBE), Universitat Politècnica de Catalunya—BarcelonaTech (UPC), Barcelona 08019, Spain; Barcelona Research Centre in Multiscale Science and Engineering, Universitat Politècnica de Catalunya—BarcelonaTech (UPC), Barcelona 08019, Spain; The Barcelona Institute of Science and Technology, Institute for Bioengineering of Catalonia (IBEC), 08028 Barcelona, Spain;* orcid.org/0000-0003-4462-6075

Complete contact information is available at: https://pubs.acs.org/10.1021/acsapm.6c00875

Author Contributions

F.C.: Methodology, Investigation, Data curation, Formal analysis, Writing—original draft, Writing—review and editing; F.S.P.: Writing—review and editing, Funding acquisition, Supervision; C.F.: Writing—review and editing, Conceptualization (WPU design); Funding acquisition (WPU synthesis and characterization); G.P.: Writing—review and editing, Conceptualization (WPU design), Funding acquisition (WPU synthesis and characterization); M.M.P.M.: Investigation (mechanical assays development), Writing—review and editing, Funding acquisition; C.A.: Writing—review and editing, Funding acquisition; L.R.: Writing—original draft, Writing—review and editing, Methodology, Investigation, Data curation, Formal analysis, Visualization, Supervision, Conceptualization, Validation.

Notes

The authors declare no competing financial interest.

■ ACKNOWLEDGMENTS

This publication is part of the I + D + i project PID2021-125257OB-I00 and CEX2023-001300 M funded by MCIN/AEI/10.13039/501100011033. Authors would like to thank the Agència de Gestió d'Ajuts Universitaris i de Recerca (2021 SGR 00387) for financial support. Support for the research of C.A. was also received through the prize "ICREA Academia" for excellence in research funded by the Generalitat de Catalunya. This work was also founded by the Italian "Ministero dell'Università e della Ricerca" MUR (FFR-D15-161199 and PJ_DR_D15_INCR10_38_528421_CANCIL-LA) and by RD15-P5ERISS_MARGINE.

■ REFERENCES

(1) Peter, S.; Khwaza, V.; Alven, S.; Naki, T.; Aderibigbe, B. A.; et al. PEGylated nanoliposomes encapsulated with anticancer drugs for breast and prostate cancer therapy: An update. *Pharmaceutics* **2025**, *17*, 20190.

(2) Pardella, E.; Pranzini, E.; Nesi, I.; Parri, M.; Spatafora, P.; Torre, E.; et al. Therapy-induced stromal senescence promoting aggressiveness of prostate and ovarian cancer. *Cells* **2022**, *11*, 4026.

(3) Dragu, D. L.; Necula, L. G.; Bleotu, C.; Diaconu, C. C.; Chivu-Economescu, M. Therapies targeting cancer stem cells: Current trends and future challenges. *World J. Stem Cells* **2015**, *7*, 1185−1196.

(4) Holohan, C.; van Schaeybroeck, S.; Longley, D. B.; Johnston, P. G. Cancer drug resistance: An evolving paradigm. *Nat. Rev. Cancer* **2013**, *13*, 714−726.

(5) Gupta, S.; Gupta, P. K.; Dharanivasan, G.; Verma, R. S. Current prospects and challenges of nanomedicine delivery in prostate cancer therapy. *Nanomedicine* **2017**, *12*, 2675−2692.

(6) Roubaud, G.; Liaw, B. C.; Oh, W. K.; Mulholland, D. J. Strategies to avoid treatment-induced lineage crisis in advanced prostate cancer. *Nat. Rev. Clin. Oncol.* **2017**, *14*, 269−283.

(7) Zhong, H.; Zhou, S.; Yin, S.; Qiu, Y.; Liu, B.; Yu, H. Tumor microenvironment as niche constructed by cancer stem cells: Breaking the ecosystem to combat cancer. *J. Adv. Res.* **2025**, *71*, 279−296.

(8) Jin, Z.; Wang, Y.; Han, M.; Wang, L.; Lin, F.; Jia, Q.; et al. Tumor microenvironment-responsive size-changeable and biodegradable HA-CuS/MnO_2 nanosheets for MR imaging and synergistic chemodynamic therapy/phototherapy. *Colloids Surf. B Biointerfaces* **2024**, *238*, 113921.
(9) Yang, R.; Chen, L.; Wang, Y.; Zhang, L.; Zheng, X.; Yang, Y.; et al. Tumor microenvironment responsive metal nanoparticles in cancer immunotherapy. *Front. Immunol.* **2023**, *14*, 1237361.
(10) Zhang, D.; Zhao, Y.; Guo, D. Application and potential of the tumor microenvironment, ferroptosis, cuproptosis, and disulfidptosis in cancer treatment and monitoring. *Crit. Rev. Oncol. Hematol.* **2026**, *218*, 105066.
(11) Zhang, T. Q.; Lv, Q. Y.; Jin, W. L. The cellular-centered view of hypoxia tumor microenvironment: Molecular mechanisms and therapeutic interventions. *Biochim. Biophys. Acta, Rev. Cancer* **2024**, *1879*, 189137.
(12) Resina, L.; Esteves, T.; Ferreira, F. C.; Alemán, C. Recent advances in smart materials for cancer therapy. *J. Phys. D: Appl. Phys.* **2025**, *58*, 463001.
(13) Cancilla, F.; Martorana, A.; Fiorica, C.; Pitarresi, G.; Craparo, E. F.; Drago, S. E.; Palumbo, F. S. Development and characterization of injectable, bioadhesive, pH-responsive hyaluronic acid-based hydrogels for enhanced postoperative cancer therapy. *Int. J. Pharm.* **2025**, *685*, 126233.
(14) Kennedy, L.; Sandhu, J. K.; Harper, M. E.; Cuperlovic-Culf, M. Role of glutathione in cancer: From mechanisms to therapies. *Biomolecules* **2020**, *10*, 1429.
(15) Niu, B.; Liao, K.; Zhou, Y.; Wen, T.; Quan, G.; Pan, X.; et al. Application of glutathione depletion in cancer therapy: Enhanced ROS-based therapy, ferroptosis, and chemotherapy. *Biomaterials* **2021**, *277*, 121110.
(16) Marini, H. R.; Facchini, B. A.; Di Francia, R.; Freni, J.; Puzzolo, D.; Montella, L.; et al. Glutathione: Lights and shadows in cancer patients. *Biomedicines* **2023**, *11*, 2226.
(17) Valenti, G. E.; Tasso, B.; Traverso, N.; Domenicotti, C.; Marengo, B. Glutathione in cancer progression and chemoresistance: An update. *Redox Exp. Med.* **2023***1*e220023.
(18) Dias, D.; Resina, L.; Ferreira, F. C.; Sanjuan-Alberte, P.; Esteves, T. Synthesis strategies and cancer therapy applications of PEDOT nanoparticles. *Mater. Adv.* **2024**, *5*, 7561.
(19) Jones, C. F.; Resina, L.; Ferreira, F. C.; Sanjuan-Alberte, P.; Esteves, T. Conductive core-shell nanoparticles: Synthesis and applications. *J. Phys. Chem. C* **2024**, *128*, 11083−11100.
(20) Resina, L.; Garrudo, F. F. F.; Alemán, C.; Esteves, T.; Ferreira, F. C. Wireless electrostimulation for cancer treatment: An integrated nanoparticle/coaxial fiber mesh platform. *Biomater. Adv.* **2024**, *160*, 213830.
(21) Resina, L.; Caballero, P.; Guggenbiller, G.; Weems, A. C.; Pérez-Madrigal, M. M.; Alemán, C. Multifunctional scaffold biosensor and drug delivery system for bacterial infection prevention during skin wound healing. *Macromol. Biosci.* **2025**, *25*, No. e00247.
(22) Resina, L.; El Hauadi, K.; Sans, J.; Esteves, T.; Ferreira, F. C.; Pérez-Madrigal, M. M.; et al. Electroresponsive and pH-sensitive hydrogel as carrier for controlled chloramphenicol release. *Biomacromolecules* **2023**, *24*, 1432−1444.
(23) Resina, L.; Esteves, T.; Pérez-Rafael, S.; García, J. I. H.; Ferreira, F. C.; Tzanov, T.; et al. Dual electro-/pH-responsive nanoparticle/hydrogel system for controlled delivery of anticancer peptide. *Biomater. Adv.* **2024**, *162*, 213925.
(24) Ramírez-Alba, M. D.; Resina, L.; Garcia-Torres, J.; Macovez, R.; Alemán, C.; Pérez-Madrigal, M. M. Thiol-yne crosslinked alginate click-hydrogel for the electrical stimulation of skin wound healing. *Int. J. Biol. Macromol.* **2025**, *322*, 146880.
(25) Castrejón-Comas, V.; Mataró, N.; Resina, L.; Zanuy, D.; Nuñez-Aulina, Q.; Sánchez-Morán, J.; et al. Electro-responsive hyaluronic acid-based click-hydrogels for wound healing. *Carbohydr. Polym.* **2025**, *348*, 122941.
(26) El Hauadi, K.; Resina, L.; Zanuy, D.; Esteves, T.; Ferreira, F. C.; Pérez-Madrigal, M. M.; et al. Dendritic self-assembled structures from therapeutic charged pentapeptides. *Langmuir* **2022**, *38*, 12905−12914.
(27) Cancilla, F.; Martorana, A.; Fiorica, C.; Pitarresi, G.; Giammona, G.; Palumbo, F. S. Glutathione-integrated waterborne polyurethanes: Aqueous dispersible, redox-responsive biomaterials for cancer drug delivery. *Eur. Polym. J.* **2025**, *226*, 113759.
(28) Martorana, A.; Puleo, G.; Miceli, G. C.; Cancilla, F.; Licciardi, M.; Pitarresi, G.; et al. Redox/NIR dual-responsive glutathione extended polyurethane urea electrospun membranes for synergistic chemo-photothermal therapy. *Int. J. Pharm.* **2025**, *669*, 125108.
(29) Cancilla, F.; Cimino, M.; Martorana, A.; Fiorica, C.; Craparo, E. F.; Tinnirello, R.; Carbone, C.; Pitarresi, G.; Miceli, V.; Palumbo, F. S. Injectable redox-responsive glutathione-polyurethane/hyaluronic acid hybrid hydrogel for controlled chemotherapy in patient-derived pancreatic cancer organoids. *Mater. Today Chem.* **2025**, *50*, 103211.
(30) Fan, Z.; Pan, X.; Gu, Z.; Gao, Y.; Gao, X.; Pan, L.; Gao, W.; Jiang, D. Highly conductive and mechanically robust PEDOT:PSS-based fibers: Fabrication methods, structure−property relations, and potential applications. *Macromol. Rapid Commun.* **2025**, *46*, No. e00639.
(31) Guex, A. G.; Puetzer, J. L.; Armgarth, A.; Littmann, E.; Stavrinidou, E.; Giannelis, E. P.; Malliaras, G. G.; Stevens, M. M. Highly porous scaffolds of PEDOT:PSS for bone tissue engineering. *Acta Biomater.* **2017**, *62*, 91−101.
(32) Correa, S.; Grosskopf, A. K.; Lopez Hernandez, H.; Chan, D.; Yu, A. C.; Stapleton, L. M.; Appel, E. A. Translational applications of hydrogels. *Chem. Rev.* **2021**, *121*, 11385−11457.
(33) Duzcukoglu, H.; Kaybal, H. B.; Asmatulu, R. Enhancing the coating durability and electrical stability of fiber composites with SPEEK/PEDOT:PSS permanent coatings: A novel approach. *Polym. Degrad. Stab.* **2024**, *228*, 110908.
(34) Sau, S.; Kundu, S. Improved electrical and mechanical properties of highly stretchable polymeric films prepared by blending DMF with the mixed solution of PEDOT:PSS and PVA. *Colloids Surf., A* **2023**, *664*, 131082.
(35) Yang, Y.; Deng, H.; Fu, Q. Recent progress on PEDOT:PSS based polymer blends and composites for flexible electronics and thermoelectric devices. *Mater. Chem. Front.* **2020**, *4*, 3130−3152.
(36) Tseng, Y. T.; Lin, Y. C.; Shih, C. C.; Hsieh, H. C.; Lee, W. Y.; Chiu, Y. C.; Chen, W. C. Morphology and properties of PEDOT:PSS/soft polymer blends through hydrogen bonding interaction and their pressure sensor application. *J. Mater. Chem. C* **2020**, *8*, 6013−6024.
(37) Hoyt, K.; Castaneda, B.; Zhang, M.; Nigwekar, P.; Di Sant'Agnese, P. A.; Joseph, J. V.; Strang, J.; Rubens, D. J.; Parker, K. J. Tissue elasticity properties as biomarkers for prostate cancer. *Cancer Biomark* **2008**, *4*, 213−225.
(38) Choi, H.; Choi, W. S.; Jeong, J. O. A review of advanced hydrogel applications for tissue engineering and drug delivery systems as biomaterials. *Gels* **2024**, *10*, 693.
(39) Rajan, L.; Sidheekha, M. P.; Shabeeba, A.; Otero, T. F.; Ismail, Y. A. Structural electrochemistry of poly(3,4-ethylenedioxythiophene) and its applicability as simultaneous sensor of environmental surroundings. *J. Mater. Chem. A* **2024**, *12*, 4583−4600.
(40) Guex, A. G.; Puetzer, J. L.; Armgarth, A.; Littmann, E.; Stavrinidou, E.; Giannelis, E. P.; Malliaras, G. G.; Stevens, M. M. Highly porous scaffolds of PEDOT:PSS for bone tissue engineering. *Acta Biomater.* **2017**, *62*, 91−101.
(41) Su, Z.; Jin, Y.; Wang, H.; Li, Z.; Huang, L.; Wang, H. PEDOT:PSS and its composites for flexible supercapacitors. *ACS Appl. Energy Mater.* **2022**, *5*, 11915−11932.
(42) Xu, Z.; Xu, Y.; Qiu, Y.; et al. Pressurized organic electrodes enable practical and extreme batteries. *Nat. Commun.* **2025**, *16*, 4561.
(43) Rivnay, J.; Mannsfeld, S. C. B.; Miller, C. E.; Salleo, A.; Toney, M. F. Quantitative determination of organic semiconductor microstructure from the molecular to device scale. *Chem. Rev.* **2012**, *112*, 5488−5519.

https://doi.org/10.1021/acsapm.6c00875
ACS Appl. Polym. Mater. 2026, 8, 8479−8494

(44) Fan, T.; Jian, L.; Liu, C.; et al. Controlled synthesis of quasi one-dimensional graphene nanostructure for high performance supercapacitor. *Synth. Met.* **2022**, *289*, 117131.
(45) Bansal, M.; Dravid, A.; Aqrawe, Z.; Montgomery, J.; Wu, Z.; Svirskis, D. Conducting polymer hydrogels for electrically responsive drug delivery. *J. Controlled Release* **2020**, *328*, 192−209.
(46) Karande, T. S.; Ong, J. L.; Agrawal, C. M. Diffusion in musculoskeletal tissue engineering scaffolds: Design issues related to porosity, permeability, architecture, and nutrient mixing. *Ann. Biomed. Eng.* **2004**, *32*, 1728−1743.
(47) Loh, Q. L.; Choong, C. Three-dimensional scaffolds for tissue engineering applications: Role of porosity and pore size. *Tissue Eng., Part B* **2013**, *19*, 485−502.
(48) Agemy, L.; Sugahara, K. N.; Kotamraju, V. R.; Gujraty, K.; Girard, O. M.; Kono, Y.; Mattrey, R. F.; Park, J. H.; Sailor, M. J.; Jimenez, A. I.; et al. Nanoparticle-induced vascular blockade in human prostate cancer. *Blood* **2010**, *116*, 2847−2856.
(49) Zanuy, D.; Sayago, F. J.; Revilla-López, G.; Ballano, G.; Agemy, L.; Kotamraju, V. R.; Jiménez, A. I.; Cativiela, C.; Nussinov, R.; Sawvel, A. M.; et al. Engineering strategy to improve peptide analogs: From structure-based computational design to tumor homing. *J. Comput.-Aided Mol. Des.* **2013**, *27*, 31−43.
(50) Zhang, B.; Wang, H.; Shen, S.; She, X.; Shi, W.; Chen, J.; Zhang, Q.; Hu, Y.; Pang, Z.; Jiang, X. Fibrin-targeting peptide CREKA-conjugated multi-walled carbon nanotubes for self-amplified photothermal therapy of tumor. *Biomaterials* **2016**, *79*, 46−55.
(51) Remant Bahadur, K. C.; Chandrashekaran, V.; Cheng, B.; Chen, H.; Peña, M. M. O.; Zhang, J.; Montgomery, J.; Xu, P. Redox potential ultrasensitive nanoparticle for the targeted delivery of camptothecin to HER2-positive cancer cells. *Mol. Pharmaceutics* **2014**, *11*, 1897−1905.
(52) Liu, J.; Huang, W.; Pang, Y.; Huang, P.; et al. Molecular self-assembly of a homopolymer: An alternative to fabricate drug-delivery platforms for cancer therapy. *Angew. Chem., Int. Ed.* **2011**, *50*, 9162−9166.
(53) Hettiarachchi, S. D.; Kirbas Cilingir, E.; Maklouf, H.; Seven, E. S.; Paudyal, S.; Vanni, S.; Graham, R. M.; Leblanc, R. M. pH and redox triggered doxorubicin release from covalently linked carbon dots conjugates. *Nanoscale* **2021**, *13*, 5507−5518.
(54) Zhang, S.; Guo, N.; Wan, G.; et al. pH and redox dual-responsive nanoparticles based on disulfide-containing poly(β-amino ester) for combining chemotherapy and COX-2 inhibitor to overcome drug resistance in breast cancer. *J. Nanobiotechnol.* **2019**, *17*, 109.
(55) Cao, Y.; Gao, M.; Chen, C.; Fan, A.; et al. Triggered-release polymeric conjugate micelles for on-demand intracellular drug delivery. *Nanotechnology* **2015**, *26*, 115101.
(56) Accardo, P.; Cancilla, F.; Martorana, A.; Calascibetta, F.; Amico, G.; Pitarresi, G.; Fiorica, C.; Chinnici, C. M.; Palumbo, F. S. Eco-friendly fabrication of secretome-loaded, glutathione-extended waterborne polyurethane nanofibers. *Int. J. Mol. Sci.* **2025**, *26*, 11556.
(57) Hu, F.; Xue, Y.; Xu, J.; Lu, B. PEDOT-based conducting polymer actuators. *Front. Robot. AI* **2019**, *6*, 114.
(58) Park, H. S.; Ko, S. J.; Park, J. S.; Kim, J. Y.; Song, H. K. Redox-active charge carriers of conducting polymers as a tuner of conductivity and its potential window. *Sci. Rep.* **2013**, *3*, 2454.
(59) Alessandri, I.; Torricelli, F.; Cerea, B.; Speziani, M.; Romele, P.; Kovacs-Vajna, Z. M.; Vassalini, I. Why PEDOT:PSS should not be used for Raman sensing of redox states (and how it could be). *ACS Appl. Mater. Interfaces* **2022**, *14*, 56363−56373.
(60) Sanviti, M.; Martínez-Tong, D. E.; Rebollar, E.; Ezquerra, T. A.; García-Gutiérrez, M. C. Crystallization and phase separation in PEDOT:PSS/PEO blend thin films: Influence on mechanical and electrical properties. *Polymer* **2022**, *262*, 125475.
(61) Teixeira do Nascimento, A.; Stoddart, P. R.; Goris, T.; Kael, M.; Manasseh, R.; Alt, K.; Tashkandi, J.; Kim, B. C.; Moulton, S. E. Stimuli-responsive materials for biomedical applications. *Adv. Mater.* **2025**, *37*, No. e07559.
(62) Goswami, I.; Perry, J. B.; Allen, M. E.; Brown, D. A.; von Spakovsky, M. R.; Verbridge, S. S. Influence of pulsed electric fields and mitochondria−cytoskeleton interactions on cell respiration. *Biophys. J.* **2018**, *114*, 2951−2964.
(63) Nikolić, N.; Skaret Bakke, S.; Tranheim Kase, E.; Rudberg, I.; Flo Halle, I.; Rustan, A. C.; Thoresen, G. H.; Aas, V. Electrical pulse stimulation of cultured human skeletal muscle cells as an in vitro model of exercise. *PLoS One* **2012**, *7*, No. e33203.
(64) Pérez-Nava, A.; González-Campos, J. B.; Frontana-Uribe, B. A. Conducting polymers for in situ drug release triggered via electrical stimulus. *ACS Appl. Polym. Mater.* **2024**, *6*, 9375−9395.
(65) Mycielska, M. E.; Djamgoz, M. B. A. Citrate transport in the human prostate epithelial PNT2-C2 cell line: Electrophysiological analyses. *J. Physiol.* **2004**, *559*, 821−833.
(66) Mycielska, M. E.; Palmer, C. P.; Brackenbury, W. J.; Djamgoz, M. B. A. Expression of Na+-dependent citrate transport in a metastatic human prostate cancer cell line and regulation by voltage-gated Na+ channel activity. *J. Physiol.* **2005**, *563*, 393−408.

https://doi.org/10.1021/acsapm.6c00875
ACS Appl. Polym. Mater. 2026, 8, 8479−8494